



HAL
open science

Conversion of snail shells (*Achatina achatina*) acclimatized in Benin to calcium phosphate for medical and engineering use

Sidoine Bonou, Etienne Sagbo, Clémentine Aubry, Cédric Charvillat, Besim
Ben-Nissan, Sophie Cazalbou

► To cite this version:

Sidoine Bonou, Etienne Sagbo, Clémentine Aubry, Cédric Charvillat, Besim Ben-Nissan, et al.. Conversion of snail shells (*Achatina achatina*) acclimatized in Benin to calcium phosphate for medical and engineering use. *Journal of The Australian Ceramic Society*, 2019, 55 (4), pp.1177-1186. 10.1007/s41779-019-00334-6 . hal-02505628

HAL Id: hal-02505628

<https://hal.science/hal-02505628>

Submitted on 11 Mar 2020

HAL is a multi-disciplinary open access archive for the deposit and dissemination of scientific research documents, whether they are published or not. The documents may come from teaching and research institutions in France or abroad, or from public or private research centers.

L'archive ouverte pluridisciplinaire **HAL**, est destinée au dépôt et à la diffusion de documents scientifiques de niveau recherche, publiés ou non, émanant des établissements d'enseignement et de recherche français ou étrangers, des laboratoires publics ou privés.



Open Archive Toulouse Archive Ouverte (OATAO)

OATAO is an open access repository that collects the work of Toulouse researchers and makes it freely available over the web where possible

This is an author's version published in: <http://oatao.univ-toulouse.fr/25561>

Official URL: <https://doi.org/10.1007/s41779-019-00334-6>

To cite this version:

Bonou, Sidoine and Sagbo, Etienne and Aubry, Clémentine  and Charvillat, Cédric  and Ben-Nissan, Besim and Cazalbou, Sophie 
Conversion of snail shells (Achatina achatina) acclimatized in Benin to calcium phosphate for medical and engineering use. (2019) Journal of the Australian Ceramic Society, 55 (4). 1177-1186. ISSN 2510-1560

Any correspondence concerning this service should be sent to the repository administrator: tech-oatao@listes-diff.inp-toulouse.fr

Conversion of snail shells (*Achatina achatina*) acclimatized in Benin to calcium phosphate for medical and engineering use

S. A. S Bonou¹ · E. Sagbo¹ · C. Aubry^{2,3} · C. Charvillat² · B. Ben-Nissan⁴ · S. Cazalbou²

Abstract

Most methods for producing calcium phosphates involve synthetic calcium and phosphates sources. However, it has recently been proposed that calcium phosphate can be produced with bio-based calcium sources such as nacre, coral, and cuttlefish bones. One specific source of bio-based calcium is found in the *Achatina* snail shell, which becomes a waste product after flesh consumption. The present work aimed to assess the effectiveness of *Achatina* snail shells and to study the conversion kinetics in both acid and alkaline environment rich in phosphate ions. It was observed that in acidic conditions, the calcium released by the dissolution of the aragonite precipitates with the phosphate ions of reaction medium induces brushite formation which is rapidly converted into monetite. In alkaline conditions, calcium released from aragonite reacts with surrounding phosphates and carbonate ions and induces carbonated apatite precipitation. Regardless of the source of calcium used in the presence of phosphate, the conversion is carried out according to complex phenomena that involve topotactic transformation or dissolution-precipitation mechanisms.

Keywords Calcium phosphate · Calcium carbonate · Snail shell · Chemical conversion · XRD · FTIR

Introduction

Historically, natural products such as wood, gold, and coral were some of the first materials used to repair human bones. Today, these products remain a source of inspiration for modern researchers in the field of biomaterials. Several research initiatives have focused on exploring new possible materials for the production of calcium phosphate [1–7]. One promising biosourced material is coral. Indeed, coral shows promise due to its porous structure which is similar to cancellous bone, its chemical composition which provides the calcium ions necessary for the precipitation of neoformed bone, and its

bioactive ions such as magnesium and strontium that promote the activity of osteoblasts responsible for bone regeneration [8–11]. It is the reason why many articles treat on the use of coral in bone repair surgery and recent studies have focused on the conversion of calcium carbonate coral to calcium phosphate to promote bone regeneration [6, 12–15]. Regardless of the source of calcium used in the presence of phosphate, the conversion is carried out according to complex phenomena that involve topotactic transformation or dissolution-precipitation mechanisms that lead to the formation of different phases: monetite (DCPA), brushite (DCPD), octacalcium phosphate (OCP), hydroxyapatite deficiency (DHA), hydroxyapatite (HA), or tricalcium phosphate (TCP). The phases formed then depend on the experimental conditions. The main conditions influencing precipitation of calcium phosphate are phosphate and calcium concentrations, pH, temperature, ionic strength, the presence of other ions, and reaction duration. Table 1 summarizes the various calcium phosphates formed, taking into account the temperature and pH parameters.

Recently, *Achatina achatina* snails have been considered a promising material with which calcium phosphate can be produced. As such, the current study explored the possibility of converting *Achatina* snail shells, which constitute a “noble”

✉ S. Cazalbou
sophie.cazalbou@univ tlse3.fr

¹ Laboratoire de Chimie Inorganique et de l'Environnement (LACIE) FAST, UAC, Cotonou, Bénin

² CIRIMAT Camot Institute, UPS INPT CNRS UMR 5085, University of Toulouse, Toulouse, France

³ Laboratoire de Génie Chimique, UMR 5503, INPT, Université de Toulouse 3, Toulouse, France

⁴ Department of Chemistry and Forensic Science, University of Technology Sydney, Broadway, NSW 2007, Australia

Table 1 The characteristics of calcium phosphate phases formed in different physicochemical conditions

Name	Chemical formula	25 °C	37 °C	60 °C	80 °C
DCPD	CaHPO ₄ · 2H ₂ O	pH 4–6 [16]	pH 4–6 [16]	pH 4 [17]	
DCPA	CaHPO ₄		pH 4–6 [18]	pH 6.5 [19]	pH 6.5 [19]
OCP	Ca ₈ H ₂ (PO ₄) ₆ · 5H ₂ O		pH 6.5 [20]	pH 5 [20]	pH 4 [20]
Hap	Ca ₁₀ (PO ₄) ₆ (OH) ₂	pH 5–9 [18, 21]	pH 5–8.5 [22]	pH 7–9 [21]	pH 6–9 [21]

waste, to calcium phosphate using the simply wet chemical method. Moreover, the kinetics of conversion was investigated. The morphology and evolution of the crystalline phases were analyzed over a period of 24 h, taking into account the reaction media used and in particular their pH.

Materials and methods

Material

The raw materials used for the current study were the shells of *Achatina achatina* snails. After washing and rinsing with distilled water, the shells were crushed in a mortar and then crushed in a mill. Then, the powder was sieved in a 1-mm sieve. The diameter of the resulting powder was less than 1 mm. Figure 1 shows the stages of powder production.

Methods

Conversion of *Achatina* snail shells to calcium phosphate

In order to follow the conversion of snail shells to calcium phosphate, two solutions containing phosphate were prepared to obtain phosphate acid and alkaline media. The two solutions of reagent (acid reagent A: H₃PO₄ and alkaline reagent B: (NH₄)₂HPO₄) were prepared either by mixing 5 mL of orthophosphoric acid (85% by weight) or by dissolving 6.67 g of diammonium hydrogen phosphate in 325 mL of deionized water. Then, 6 g of snail shell powder was added to the prepared solutions, stirred at 540 rpm, and maintained at 80 ± 0.5 °C for 24 h. The Ca/P solution ratios were chosen so that under given pH conditions (acidic or alkaline pH), the

sub-saturation of solutions avoids the simultaneous precipitation of two phosphocalcic phases and allow to follow the evolution of the conversion of the snail shells.

Thus, at acidic pH, the Ca/P = 0.72 ratio was lower than those of the brushite or the monetite (Ca/P = 1). Similarly, at alkaline pH, the ratio Ca/P = 1.16 was lower than those of OCP (1.33) and HA (1.667) which preferentially precipitate at these pH values. At 0.5 h, 1.5 h, 2.5 h, 3.5 h, 4.5 h, and 24 h, an equal volume of the suspension was taken from the reaction medium. The samples were filtered, washed with deionized water, and dried at 37 ± 0.5 °C for 15 h. The products obtained from conversions carried out in the acid medium were denoted EG-A 0.5 h, EG-A 1.5 h, EG-A 2.5 h, EG-A 3.5 h, EG-A 4.5 h, and EG-A 24 h. The products obtained from conversions carried out in the alkaline medium were denoted EG-B 0.5 h, EG-B 1.5 h, EG-B 2.5 h, EG-B 3.5 h, EG-B 4.5 h, and EG-B 24 h. Details of the composition of the reaction media and the corresponding ratios Ca/P and Ca/(P + C) are shown in Table 2.

Phase analysis by XRD

Phase analysis of the products was carried out via the X-ray powder diffraction method using D8 ADVANCE (BRUKER), under Cu K α 1 + 2 = 0.15418 nm radiation, from 20 to 80° (2 theta), steps of 0.02°, 2 s/step, divergence slit 0.3°, Sollers slit 2.5°, and detector linear LynxEye (2.73°). The phase quantification was done using Rietveld analysis performed by Topas software (3.0v).

Morphology by SEM

The observations of the morphology of unconverted and converted snail shells were made with a scanning electron



Fig. 1 Photos of some steps of powdering snail shells

Table 2 Composition of acid and alkaline reaction media and corresponding Ca/P and Ca/(P + C) ratios

	Conversion in acid medium		Conversion in alkaline medium	
	325 mL of water		325 mL of water	
Volume of solution	325 mL of water		325 mL of water	
Reagent	Shells (EG)	H ₃ PO ₄ (85%)	Shells (EG)	(NH ₄) ₂ HPO ₄
Amount of reagent	6 g	5 mL	6 g	6.67 g
Molar ratio Ca/P	0.72		1.16	
Molar ratio Ca/(P + C)	0.42		0.54	

microscope (SEM, Leo 435 VP, LEICA Microsystems (Cambridge, U.K.)). The acceleration voltage was set at 5 kV, the probe current at 50 pA, and the diaphragm at 30 μ m. The samples were metalized with silver (9 nm) prior to observation.

FTIR analysis

The synthesized calcium phosphate powders were ground in an agate mortar and thoroughly mixed with KBr (FTIR Grade). Three milligrams of powder sample was mixed with 300 mg of KBr powder (1% w/w). Transparent pellets were prepared in a stainless steel die by applying a uniaxial load of a 6.89-MPa pressure (Carver press). The FTIR spectra were acquired by transmission, in the wavenumber range 400–4000 cm^{-1} using a Nicolet 5700 spectrometer (64 scans, with a resolution of 4 cm^{-1}). The spectra were subsequently analyzed with the OMNIC 8 software (Thermo Nicolet).

Dataavailability Available Online at www.austceram.com/category/journal/.

Results and discussions

Results

Characterization of unconverted *Achatina achatina* shells

TGA and chemical composition The results of chemical composition, shown in Table 3, were obtained by X-ray fluorescence using the fusion method based on the realization of pearls.

On the TGA thermogram, O.M. is used to name “organic matter” which was present in the raw shell powder.

Main weight loss events registered during heat treatment can be assigned to water loss (20–180 $^{\circ}$ C), inter-crystalline (180–400 $^{\circ}$ C), and intra-crystalline (400–600 $^{\circ}$ C) organic matter loss and emission of CO₂ (> 600 $^{\circ}$ C) during carbonate decomposition [22, 23] (Fig. 2). From the results of TGA analysis, the organic matter in snail shells was evaluated at 2.12% (w/w). The mineral composition of the EG shells is

shown in Table 3. Results show the presence of trace elements of Mg²⁺ and Si²⁺ which are particularly interesting for biomedical application due to their ability to enhance bone cells proliferation and favor mineralization [24, 25].

Fourier transform infrared spectroscopy and XRD analysis The indexing of the represented diffractogram, by comparison of the peaks obtained with those of JCDPS database, shows that mineral phases of snail shells are calcium carbonates with aragonite as dominant phase (98.6 M%) completed with trace of calcite (1.4 M%) (JCPDS files [00-041-1475] and [00-047-1743] respectively) (Fig. 3). Due to the small amount of calcite, the characteristic bands of calcite (1404 cm^{-1} (ν_3), 872 cm^{-1} (ν_2), and 712 cm^{-1} (ν_4)) are coincident with those of aragonite (1490 cm^{-1} (ν_3), 856 cm^{-1} (ν_2), and 713 cm^{-1} (ν_4)) and therefore, the FTIR spectrum shown in Fig. 4 presents a characteristic spectrum of aragonite. Small variations in absorption bands positions were registered between pure aragonite and aragonite from snail shells. Indeed, characteristic absorptions bands of pure aragonite at 1490 cm^{-1} (ν_3), 856 cm^{-1} (ν_2), and 713 cm^{-1} (ν_4) were shifted to 1478 cm^{-1} (ν_3), 860 cm^{-1} (ν_2), and 712 cm^{-1} (ν_4). The small variations in absorption bands positions can be attributed to the presence of snail shells of organic matter (2.12% w/w) and trace elements such as magnesium, potassium, iron, aluminum, silicon, and sodium (less than 1% w/w) [26–32].

Morphology by SEM The microarchitecture of the samples was determined using SEM analysis. The SEM images of powdered snail shells highlight small needle crystals, some of which are bonded longitudinally in the same direction (Fig.

Table 3 Chemical composition of mineral elements of EG shells by fusion method of XRF

Cation elements	Mineral analysis, % (w/w)
Ca	56.52
Mg	0.61
Si	0.16
Al	0.12
Na	0.10
Fe	0.07
K	0.05

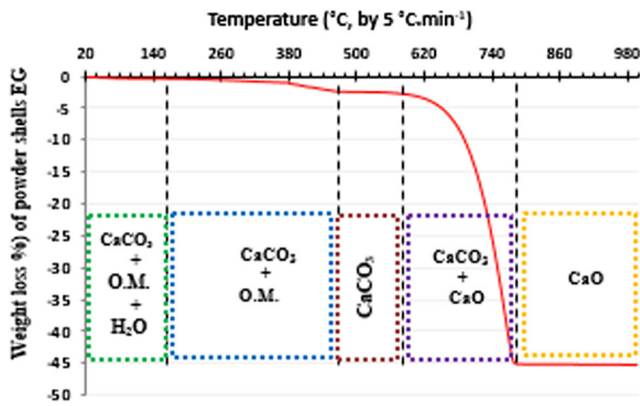


Fig. 2 TGA analysis

5). It is likely that these are linked by organic matter. For other powdered snail shells, the parallel organization was not apparent, but instead appeared randomly distributed, which is likely due to the grinding of the powder.

Characterization of *Achatina achatina* shells converted to calcium phosphate

pH measurements pH measurement solutions are made using the 765 laboratory pH meter (Knick, Germany) calibrated with two buffer solutions (acetic buffer: pH = 4 and ammonia buffer: pH = 9 at 25 °C) measurements.

During the conversion reaction of calcium carbonate to calcium phosphate, the pH was monitored and the results are shown in Fig. 6. For both EG-A and EG-B, the first pH value was measured immediately after pouring the reagent then stirred into the aqueous suspension containing the shell powder. For EG-A (acid medium), immediately after adding

Fig. 3 Diagram of X ray diffraction of *Achatina achatina* snail shells before conversion

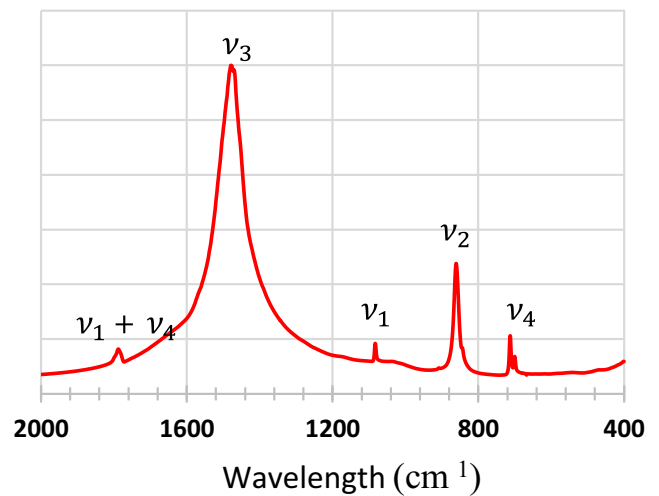
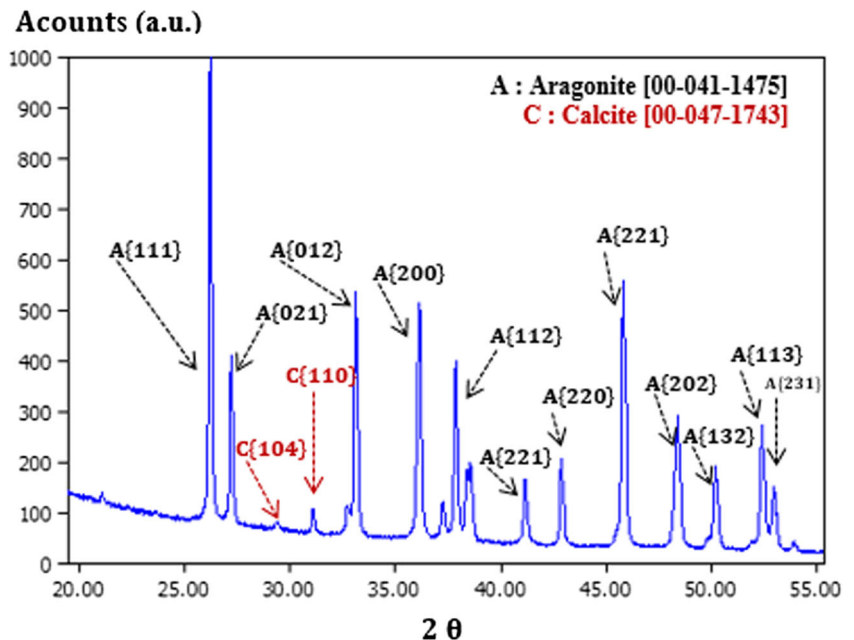


Fig. 4 Fourier transform infrared spectrum of unconverted EG shells

H₃PO₄, the pH of suspension decreased to 1.78. The pH kinetics presented in Fig. 6 can be divided into three distinct phases. The first phase consisted of a rapid increase in the pH from 1.78 to 3.03 for the first 0.5 h of the reaction. Then, the pH decreased to 2.73 after 2.5 h. Finally, in the third phase, the pH gradually increased to 3.5 at 24 h. These changes were related to the gaseous release of carbon dioxide (CO₂) and the dissolution of acid carbonate phases from aragonite during its conversion to calcium phosphate. Over time, the reduction of the carbonates present in the reaction medium led to a gradual increase of the pH.

The results for EG-B (alkaline medium) contrasted those of EG-A. Indeed, for EG-B, the pH reached 8.27 immediately after adding (NH₄)₂HPO₄ and gradually increased to 9.3 after 24 h. This gradual increase of pH can be explained by the

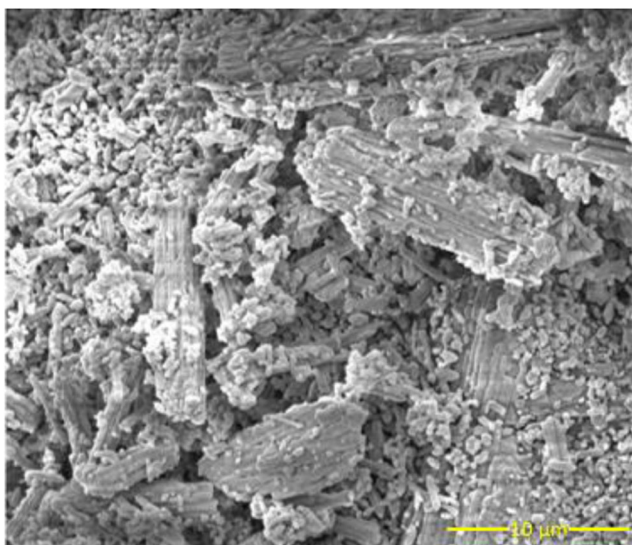


Fig. 5 SEM image of *Achatina* snail shells

releasing of carbonate ions when some of them were exchanged with phosphate ions during the reaction in the alkaline solution. The carbonate ions released in the aqueous medium reacted with water to generate hydroxide ions. These hydroxide ions are responsible for the pH increase during the reaction.

FTIR The chemical constituents of the pulverized shells for all time measurements in all experiments were analyzed by FTIR. The results are presented in Fig. 7a, b. Regardless of the reagent used, the conversion of powdered snail shells to calcium phosphates started immediately after addition of the reagents and mixing the precursor at 80 °C. For EG-A, 30 min after introduction of H_3PO_4 , the FTIR spectrum showed characteristic bands of aragonite ($\nu_3 CO_3$ at 1478 cm^{-1} , ν_2 at 860 cm^{-1} , and ν_4 at 712 cm^{-1}) as well as those of brushite (DCPD) ($\nu_3 PO_4$ at 1132 and 1060 cm^{-1} , $\nu_1 PO_4$ at 984 cm^{-1} , and $\nu_4 PO_4$ at 526 cm^{-1} [33]). After 1.5 h, the intensity of the carbonate bands decreased and the phosphate bands of the brushite gave way to the vibration bands of the phosphates characteristic of monetite (DCPA) ($\nu_3 PO_4$ at 1128 and 1064 cm^{-1} , $\nu_1 PO_4$ at 992 cm^{-1} , and $\nu_4 PO_4$ at 576 and 563 cm^{-1} [33]). As the

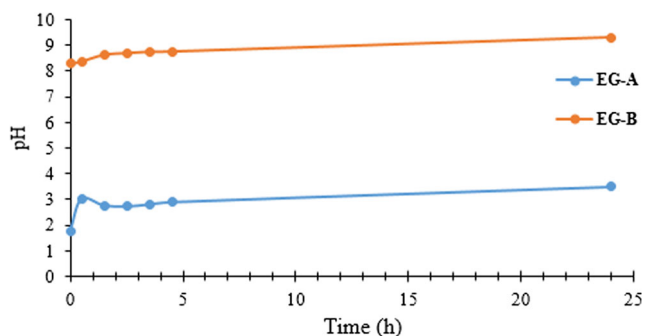


Fig. 6 pH kinetics during the reaction of conversion of calcium carbonate to calcium phosphate

reaction occurs, a decrease in the intensity of the carbonate vibration bands was observed. After 24 h, the FTIR spectrum no longer shows carbonate vibration bands and only the phosphate bands of monetite constituted the spectrum. For EG-B, an immediate decrease in the intensity of the carbonate bands of aragonite coupled with an increase in the phosphate bands of hydroxyapatite ($\nu_3 PO_4$ at 1092 and 1040 cm^{-1} , $\nu_1 PO_4$ at 962 cm^{-1} , and $\nu_4 PO_4$ at 601 and 561 cm^{-1} [33]) was recorded. Importantly, the amount of aragonite converted to hydroxyapatite during the first 2.5 h of the reaction and decreased over time. From 4.5h, the CO_3 bands of aragonite decreased to reveal the CO_3 bands of the substituted hydroxyapatite. Thus, the vibration bands at 1450 and 880 cm^{-1} can be attributed to type A carbonates (substituted for OH) and the bands at 1412 and 873 cm^{-1} to type B carbonates (substituted for PO_4^{3-}) [34, 35]. Indeed, apatite is a very “welcoming” structure in which a large number of ionic substitutions can occur. During the conversion of aragonite into apatite, the ionic species present have the possibility of integrating the freshly formed apatitic phase. Thus, some of the carbonate ions from aragonite integrate the apatite structure resulting in the formation of carbonate apatite. After 24 h of treatment, the reaction did not seem to be complete, as only 87% of the pulverized shells were converted into carbonated apatite.

XRD Figure 8 shows the X-ray diffraction diagrams and Table 4 displays the results of the phase quantifications present during the conversion process for the powders treated in an acidic environment in the presence of H_3PO_4 (EG-A) (also see Fig. 8a). Table 5 displays the results of the phase quantifications present during the conversion process for the powders treated in an alkaline environment in the presence of $(NH_4)_2HPO_4$ (EG-B) (also see Fig. 8b).

For the EG-A samples (obtained with the orthophosphoric acid), the X-ray diagrams show the evolution of three crystalline phases.

The aragonite whose intensity of their characteristics peaks decreased during the duration of the conversion; the brushite is formed in the first step of the conversion process and then transforms to monetite which is the final product obtained at the end of reaction.

The results shown in Table 5 clearly demonstrate that the first product formed in the immediate moments of the reaction was brushite. This may be due to the calcium brought by the aragonite and phosphate within the reaction medium. The second phase of conversion involved the transformation of the brushite into monetite. After 24 h, the conversion of aragonite, composed of snail shells, was complete, and the only detectable product was monetite.

Regarding the EG-B samples (obtained with $(NH_4)_2HPO_4$), Fig. 8 shows a gradual decrease of diffraction peaks of calcium carbonates, whereas there was an increase of the intensity of peaks attributed to hydroxyapatite. Table 5 demonstrates the

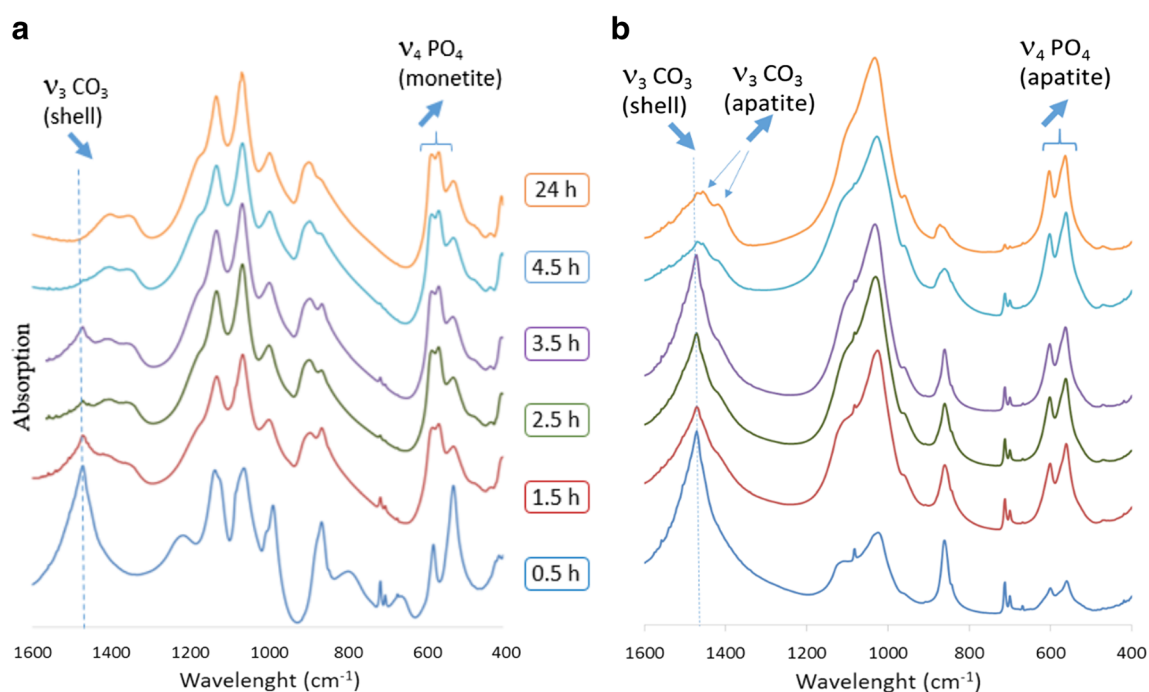


Fig. 7 **a** FTIR spectra of snail shells converted in orthophosphoric acid phosphate solution. **b** FTIR spectra of snail shells converted in ammonium phosphate solution

gradual conversion of aragonite to apatitic calcium phosphate. After 24 h, 87% of the aragonite had been converted to hydroxyapatite. Combined with the results observed from FTIR, and the width of the diffraction peaks, the current results confirm that the apatitic structure formed is not pure hydroxyapatite but poorly crystallized carbonate apatite. These results are similar to previous findings that observed conversions with coral-line structures and sea snail shells [6, 12–14, 36].

Morphology

The morphologies of the products formed after 1.5 h and 24 h of reaction are shown in Fig. 9. The results reveal the changes

in morphology over time for both the acid and alkaline reaction medium.

For EG-A, after 1.5 h of conversion in an acid medium at 80 °C, the freshly formed crystals were large thin plates affixed to massive crystals with flat surfaces. However, after 24 h, they showed a general granular morphology with no regular shaped crystalline components observed.

For EG-B, products obtained after 1.5 h of the conversion process in alkaline environment have morphology of petal-like crystals. Over time, the size of the petals decreased and their organization gave rise to an entangled structure formed of small badly defined platelets. Ducan et al. attribute this change of morphology to differences in synthesis conditions, differences of reaction medium, and different free ions

Table 4 Quantification for EG A experiment showing the amount of present phases and pH of the reaction medium

Time (h)	Ratio (% by mass) of formed phases (XRD) $\pm 0.3\%$				Physicochemical parameters
	Aragonite, CaCO ₃ (JCPDS 00 041 1475)	Calcite, CaCO ₃ (JCPDS 00 047 1743)	Brushite, CaHPO ₄ ·2H ₂ O (JCPDS 00 009 0077)	Monetite, CaHPO ₄ (JCPDS 01 070 0360)	
0	98.6 \pm 0.3	1.4 \pm 0.3	0 \pm 0.3	0 \pm 0.3	1.78 \pm 0.01
0.5	28.7 \pm 0.3	0 \pm 0.3	71.3 \pm 0.3	0 \pm 0.3	3.03 \pm 0.01
1.5	14.2 \pm 0.3	0 \pm 0.3	0 \pm 0.3	85.8 \pm 0.3	2.77 \pm 0.01
2.5	2.9 \pm 0.3	0 \pm 0.3	0 \pm 0.3	97.1 \pm 0.3	2.73 \pm 0.01
3.5	1.6 \pm 0.3	0 \pm 0.3	0 \pm 0.3	98.4 \pm 0.3	2.81 \pm 0.01
4.5	2.5 \pm 0.3	0 \pm 0.3	0 \pm 0.3	97.5 \pm 0.3	2.90 \pm 0.01
24	0.6 \pm 0.3	0 \pm 0.3	0 \pm 0.3	99.4 \pm 0.3	3.50 \pm 0.01

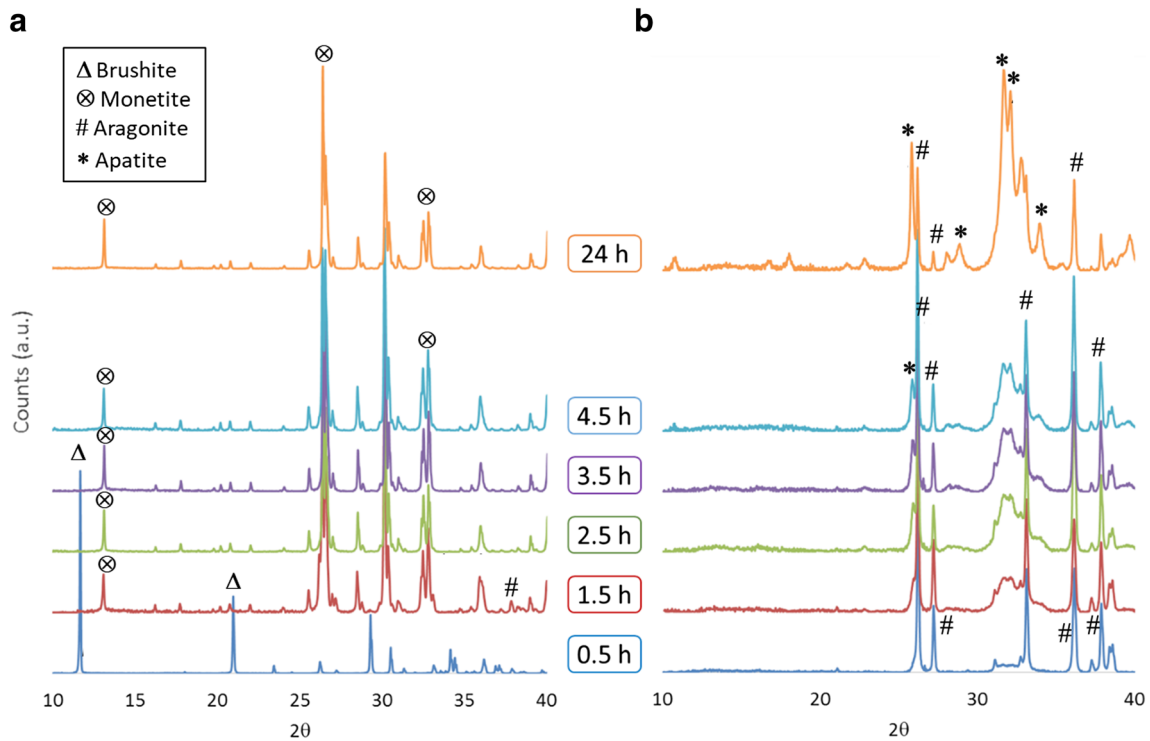


Fig. 8 **a** XRD patterns of snail shells converted in orthophosphoric acid phosphate solution. **b** XRD patterns of snail shells converted in ammonium phosphate solution

concentration in media [37], all of which were present in the current experiments.

Discussion

The present work demonstrates that calcium carbonate, which is present in snail shells, can be converted to various calcium phosphate phases. These changes were shown to depend on the reaction medium and, in particular, the pH. Mekmene et al. [38] previously demonstrated that the main factor influencing the crystalline structure of calcium phosphate precipitates is pH. Indeed, when pH

was left to drift after the addition of calcium, brushite is found to be the most prevalent crystalline phase in all precipitates.

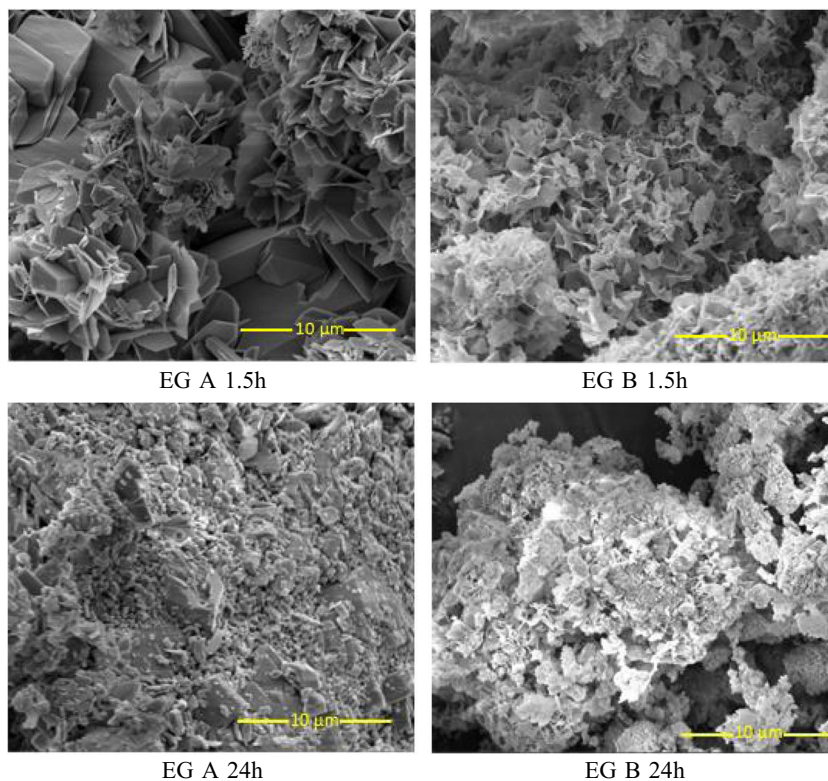
However, when pH levels are kept constant, no brushite is seen in precipitates, and there is instead the presence of low crystallized calcium-deficient apatite [38]. Although the operating conditions and the reaction media used in the present study differ from those used by Mekmene et al., the current results agree with those obtained in their work.

In considering the conversion mechanisms that can lead to the formation of phosphocalcic phases, two mechanisms are possible: dissolution-reprecipitation reactions

Table 5 Quantification for EG B experiment showing the amount of present phases and pH of the reaction medium

Time (h)	Ratio (% by mass) of formed phases (XRD) $\pm 0.3\%$			Physicochemical parameters
	Aragonite, CaCO ₃ (JCPDS 00 041 1475)	Calcite, CaCO ₃ (JCPDS 00 047 1743)	Hydroxyapatite, Ca ₁₀ (PO ₄) ₆ OH ₂ (JCPDS 00 009 0432)	
0	98.6 \pm 0.3	1.4 \pm 0.3	0	8.27 \pm 0.01
0.5	83.2 \pm 0.3	0 \pm 0.3	16.5 \pm 0.3	8.36 \pm 0.01
1.5	53.2 \pm 0.3	0 \pm 0.3	46.8 \pm 0.3	8.62 \pm 0.01
2.5	40.0 \pm 0.3	0 \pm 0.3	60 \pm 0.3	8.69 \pm 0.01
3.5	38.1 \pm 0.3	0 \pm 0.3	61.9 \pm 0.3	8.74 \pm 0.01
4.5	38.3 \pm 0.3	0 \pm 0.3	61.7 \pm 0.3	8.75 \pm 0.01
24	12.9 \pm 0.3	0 \pm 0.3	87.1 \pm 0.3	9.30 \pm 0.01

Fig. 9 SEM images showing morphology of converted products after 1.5 h and 24 h of reaction



or solid-state topotactic ion-exchange reaction mechanisms [12, 39, 40]. When the transformation involves ion-exchange mechanisms, the reaction produces pseudomorphs with crystals quite similar to the original crystals. However, the precipitation of a new phase leads to a complete modification of the organization and shape of the crystals which it is necessary to relate with the operating conditions of synthesis. Indeed, they determine the competition which can exist between the dissolution rate of the sources of calcium (here aragonite), the rate of diffusion of calcium ions, and the rate of precipitation [18, 39].

Moreover, it is important to consider how kinetic factors determine the likelihood of the formation of particular crystal phases. The formation of HAP (as deficient or substituted apatite) is much slower than that of DCPD, and during simultaneous phase formation, a larger portion of the kinetically favored phase may be observed, even though it has a smaller thermodynamic driving force. Therefore, the balance between kinetic and thermodynamic factors is important in determining the likelihood of precursor formation during calcium phosphate precipitation [6].

In this current work, the observed morphology of products from converted powdered snail shells suggests that the transformation to calcium phosphate occurs by dissolution phenomena of the early phase and then reprecipitation of the new one. Like Mekmene et al. [38], the current results suggest that the reaction mechanisms, and the final products resulting from the reactions, are strongly influenced by pH.

Orthophosphoric acid phosphate solution

Immediately after introducing snail shells into the acid medium, the pH increase was associated with a rapid dissolution of the calcium carbonate phases, which was followed by brushite precipitation. The brushite formation induced a pH change accentuated by the simultaneous release of gaseous carbon dioxide and dissolution of acidic carbonates. This was followed by the dissolution of freshly precipitated brushite and the precipitation of monetite which is the most stable phase under these conditions of pH and temperature. The gradual decrease of carbonate resulting from the dissolution of aragonite, coupled with the continued formation of monetite, led to a gradual increase in pH. Under these conditions, the solubility and rapid dissolution rate of the present phases (aragonite and calcite, then brushite) led to dissolution-reprecipitation chain reactions until a thermodynamically more stable system was obtained. The successive and rapid processes that led to the conversion of aragonite into monetite may explain the structural modifications of the crystals observed during the conversion.

Ammonium phosphate solution

In the alkaline medium, the formation of hydroxyapatite began immediately after the addition of the ammonium phosphate and the resulting pH increase. Under these conditions (pH close to 8), hydroxyapatite is the most thermodynamically

stable phase. The ability of the apatite phases to receive other ionic species than those constituting stoichiometric hydroxyapatite (sometimes accompanied by the creation of lacunae at the calcium and/or hydroxide sites) induced the precipitation of a carbonated apatite. The CO₃ ions then integrated the apatite structure by replacing some of the PO₄ ions which constituted the skeleton of the structure (B-CO₃) and a part of the OH ions located in the tunnels of apatite (A-CO₃). The presence of CO₃ ions in the phosphate sites and the hydroxide sites of apatite was confirmed by the presence of vibration bands at 1450 and 1412 cm⁻¹ in the FTIR spectra. Over time, the amount of carbonate ions increased and the formed apatite phase evolved towards a better-crystallized phase.

Conclusion

In this work, we explored the possibility of converting *Achatina achatina* snail shells to calcium phosphate using the simply wet chemical method. Moreover, we studied the kinetics of the conversion of different crystalline present phases. The current results show that *Achatina achatina* snail shells can be converted to calcium phosphate. If the conversion started immediately after introducing shell powder into the reaction media, the conversion efficiency and the final phases obtained were dependent on the reaction media, which influenced solubility and the dissolution rate of phases in this experiment. When the reaction was carried out in an acid medium (in the presence of H₃PO₄), the rapid dissolution of the calcium carbonates immediately induced brushite precipitation which constituted a transitional phase, after which dissolution finally reprecipitated as a more stable phase: monetite. When the conversion was carried out in an alkaline medium (in the presence of (NH₄)₂HPO₄), the progressive dissolution of aragonite led to the formation of poorly crystallized carbonate apatite. Then, the released carbonates integrated the phosphate sites (type B carbonates) as well as the tunnels of the apatitic structure (type A carbonates).

References

- Westbroek, P., Martin, F.: A marriage of bone and nacre. *Nature*. **392**, 861–862 (1998)
- Tadic, D., Epple, M.: A thorough physicochemical characterisation of 14 calcium phosphate based bone substitution materials in comparison to natural bone. *Biomaterials*. **25**(6), 987–994 (2004)
- Rocha, J.H.G., Lemos, A.F., Agathopoulos, S., Kannan, S., Valerio, P., Ferreira, J.M.F.: Hydrothermal growth of hydroxyapatite scaffolds from aragonite cuttlefish bones. *J Biomed Mater Res A*. **77**, 160–172 (2006)
- Lemos, A.F., Rocha, J.H.G., Quaresma, S.S.F., Kannan, S., Oktar, F.N., Agathopoulos, S., Ferreira, J.M.F.: Hydroxyapatite nano powders produced hydrothermally from nacreous material. *J Eur Ceram Soc*. **26**, 3639 (2006)
- Guo, Y.P., Yao, Y.B., Ning, C.Q., Guo, Y.J., Chu, L.F.: Fabrication of mesoporous carbonated hydroxyapatite microspheres by hydrothermal method. *Mater Lett*. **65**(14), 2205–2208 (2011)
- Ni, M., Ratner, B.D.: Nacre surface transformation to hydroxyapatite in a phosphate buffer solution. *Biomaterials*. **24**, 4323 (2003)
- Ben Nissan, B., Milev, A., Vago, R.: Morphology of sol gel derived nanocoated coralline hydroxyapatite. *Biomaterials*. **25**, 4971 (2004)
- Patat, J.L., Guillemin, G.: Natural coral used as a replacement biomaterial in bone grafts. *Ann Chir Plast Esthet*. **34**(3), 221–225 (1989)
- Damien, E., Revell, P.A.: Coralline hydroxyapatite bone graft substitute: a review of experimental studies and biomedical applications. *J Appl Biomater Biomech*. **2**, 65–73 (2004)
- He, L.Y., Zhang, X.M., Liu, B., Tian, Y., Ma, W.H.: Effect of magnesium ion on human osteoblast activity. *Braz J Med Biol Res*. **49**(7), e5257 (2016)
- Tadier, S., Bareille, R., Siadous, R., Marsan, O., Charvillat, C., Cazalbou, S., Amedee, J., Rey, C., Combes, C.: Strontium loaded mineral bone cements as sustained release systems: compositions, release properties, and effects on human osteoprogenitor cells. *J Biomed Mater Res B Appl Biomater*. **100**(2), 378–390 (2012)
- Macha, I.J., Grossin, D., Ben Nissan, B.: Conversion of marine structures to calcium phosphate materials: mechanisms of conversion using two different phosphate solutions. *Key Eng Mater*. **696**, 36–39 (2016)
- Macha, I.J., Boonyang, U., Cazalbou, S., Ben Nissan, B., Charvillat, C., Oktar, F.N., Grossin, D.: Comparative study of coral conversion, part 2: microstructural evolution of calcium phosphate. *J Aust Ceram Soc*. **51**(2), 149–159 (2015)
- Choi, G., Karacan, I., Cazalbou, S., Evans, L., Sinutok, S., Ben Nissan, B.: Conversion of calcified algae (*Halimeda* sp) and hard coral (*Porites* sp) to hydroxyapatite. *Key Eng Mater*. **758**, 157–161 (2017)
- Roy, D.M., Linnehan, S.K.: Hydroxyapatite formed from coral skeletal carbonate by hydrothermal exchange. *Nature*. **247**(5438), 220–222 (1974)
- Johnsson, M.S.A., Nancollas, G.H.: The role of brushite and octacalcium phosphate in apatite formation. *Crit Rev Oral Biol Med*. **3**, 61–82 (1992)
- Marshall, R.W., Nancollas, G.H.: The kinetics of crystal growth of dicalcium phosphate dehydrate. *J Phys Chem*. **73**(11), 3838–3844 (1969)
- Elliott, J.C.: *Structure and chemistry of the apatites and other calcium orthophosphates*. Elsevier, Amsterdam (1994)
- YoungJae, K., Seon Yong, L., Yul, R., Jinhyeok, L., Juyeun, K., Yongwoo, L., Junseok, B., Young Jae, L.: Optimizing calcium phosphates by the control of pH and temperature via wet precipitation. *J Nanosci Nanotechnol*. **15**, 10008–10016 (2015)
- LeGeros, R.Z.: Calcium phosphates in oral biology and medicine. *Monogr. Oral Sci*. **15**, 1–201 (1991)
- Chow L.C., Solubility of calcium phosphates. (eds.) *Octacalcium phosphate*, monogr. Oral Sci. Basel, Karger, vol 18. (2001), 94–111
- Rodriguez Navarro, A., Cabral de Melo, C., Batista, N., Morimoto, N., Alvarez Lloret, P., Ortega Huertas, M., Fuenzalida, V.M., Arias, J.I., Wiff, J.P., Arias, J.L.: Microstructure and crystallographic texture of giant barnacle (*Austromegabalanus psittacus*) shell. *J Structur Biol*. **156**, 355–362 (2006)
- Radishi, N.A., Mohamed, M., Yusup, S.: The kinetic model of calcination and carbonation of Anadara Granosa. *Int J Renew Energy Res*. **2**(3), 497–503 (2012)
- Wu, C., Xiao, Y., Chang, J.: Silicate based bioactive ceramics for bone regeneration application. In: Wu, C., Chang, J., Xiao, Y. (eds.) *Advanced bioactive inorganic materials for bone regeneration and*

- drug delivery, pp. 25–46. CRC Press (Taylor & Francis Group, Boca Raton (2013))
25. Burmester, A., Willumeit Römer, R., Feyerabend, F.: Behavior of bone cells in contact with magnesium implant material. *J Biomed Mater Res B Appl Biomater.* **105**(1), 165–179 (2017)
 26. Andersen, F.A., Breevi, L.J.: Infrared spectra of amorphous and crystalline calcium carbonate. *Acta Chem Scand.* **45**, 1018–1024 (1991)
 27. Fernandez, M.S., Valezuela, F., Arias, J.L., Neira Carrillo, A., Arias, J.L.: *J Struct Biol.* **196**, 187–196 (2016)
 28. Narasimhulu, K.V., Lakshamana Rao, J.: EPR and IR spectral studies of the seawater mussel *Mytilus conradinus* shells. *Spectrochim Acta A.* **56**, 1345–1353 (2000)
 29. Su, C., Suarez, D.L.: In situ infrared speciation of adsorbed carbonate on aluminum and iron oxide. *Clay Clay Miner.* **45**(6), 814–825 (1997)
 30. Addadi, L., Raz, S., Weiner, S.: Taking advantage of disorder: amorphous calcium carbonate and its roles in biomineralization. *Adv Mater.* **15**, 959–970 (2003)
 31. Coleyshaw, E.E., Crump, G., Griffith, W.P.: Vibrational spectra of the hydrated carbonate minerals ikaite, monohydrocalcite, lansfordite and nesquehonite. *Spectrochim Acta A Mol Biomol Spectrosc.* **59**(10), 2231–2239 (2003)
 32. Gueta, R., Natan, A., Addadi, L., Weiner, S., Refson, K., Kronik, L.: Local atomic order and infrared spectra of biogenic calcite. *Angew Chem Int Ed.* **46**, 291–294 (2007)
 33. Rey, C., Combes, C., Drouet, C., Grossin, D.: Bioactive ceramics: physical chemistry. In: Ducheyne, P., Healy, K., Hutmacher, D., Grainger, D.E., Kirkpatrick, J. (eds.) *Comprehensive Biomaterials*, pp. 187–221. Elsevier (2011)
 34. Borkiewicz, O., Rakovan, J., Cahill, C.L.: Time resolved in situ studies of apatite formation in aqueous solutions. *Am Mineral.* **95**(8–9), 1224–1236 (2010)
 35. Rey, C., Collins, B., Goehl, T., Dickson, I.R., Glimcher, M.J.: The carbonate environment in bone mineral: a resolution enhanced Fourier transform infrared spectroscopy study. *Calcif Tissue Int.* **45**(3), 157–164 (1989)
 36. Şahin, Y., Gündüz, O., Bulut, B., Özyeğin, L., Gökçe, H., Ağaogulları, D., Chou, J., Kayalı, E., Ben Nissan, B., Oktar, F.: Nano bioceramic synthesis from tropical sea snail shells (tiger cowrie *Cypraea Tigris*) with simple chemical treatment. *Acta Phys Pol A.* **127**(4), 1055–1058 (2015)
 37. Duncan, J., MacDonald, J.F., Hanna, J.V., Shirosaki, Y., Hayakawa, S., Osaka, A., Skakle, J.M.S., Gibson, I.R.: The role of the chemical composition of monetite on the synthesis and properties of β tricalcium phosphate. *Mater Sci Eng C.* **34**, 123–129 (2014)
 38. Mekmene, O., Quillard, S., Rouillon, T., Bouler, J.M., Piot, M., Gaucheron, F.: Effects of pH and Ca/P molar ratio on the quantity and crystalline structure of calcium phosphates obtained from aqueous solutions. *Dairy Science & Technology, EDP sciences/Springer.* **89**(3–4), 301–316 (2009)
 39. Wang, L., Nancollas, G.H.: Calcium orthophosphates: crystallization and dissolution. *Chem Rev.* **108**(11), 4628–4669 (2008)
 40. Lima, C.B.A., Airoldi, C.: Topotactic exchange and intercalation of calcium phosphate. *Solid State Sci.* **6**(11), 1245–1250 (2004)

Publisher's note Springer Nature remains neutral with regard to jurisdictional claims in published maps and institutional affiliations.